Journal of Engineering Science and Technology
Vol. 6, No. 1 (2011) 109 - 130

EFFECT OF DIFFERENT THERMAL BOUNDARY CONDITIONS AT BOTTOM WALL ON NATURAL CONVECTION IN CAVITIES

ASWATHA[1,*], C. J. GANGADHARA GOWDA[2], S. N. SRIDHARA[3], K. N. SEETHARAMU[4]

[1]Department of Mechanical Engineering, Bangalore Institute of Technology, Bangalore - 560 004, India
[2]Department of Mechanical Engineering, PES College of Engineering, Mandya - 571 401, India
[3]Principal / Director, K. S. Group of Institutions, Bangalore - 560 062, India
[4]Department of Mechanical Engineering, PES Institute of Technology, Bangalore - 560 085, India
*Corresponding Author: aswath_bit@yahoo.co.in

Abstract

Natural convection in cavities is studied numerically using a finite volume based computational procedure. The enclosure used for flow and heat transfer analysis has been bounded by adiabatic top wall, constant temperature cold vertical walls and a horizontal bottom wall. The bottom wall is subjected to uniform / sinusoidal / linearly varying temperatures. Nusselt numbers are computed for Rayleigh numbers (Ra) ranging from 10^3 to 10^7 and aspect ratios (H/L) of 1 to 3. Results are presented in the form of stream lines, isotherm plots and average Nusselt numbers. It is observed from this study that the uniform temperature at the bottom wall gives higher Nusselt number compared to the sinusoidal and linearly varying temperature cases. The average Nusselt numbers increases monotonically with Rayleigh number for aspect ratios 1, 2 and 3 for bottom wall and side walls. For the case of aspect ratios 2 and 3, the average Nusselt number for a given Rayleigh number increases at the bottom wall as compared to that for aspect ratio 1. However the average Nusselt number decreases as the aspect ratio increases from 1 to 3 for side wall.

Keywords: Natural convection, Cavities, Aspect ratio, Thermal boundary conditions, Numerical heat transfer.

Nomenclatures

AR	Aspect ratios, H/L
g	Acceleration due to gravity, m/s^2
H	Height of the cavity, m
k	Thermal conductivity, W/m K
L	Length of the cavity, m
Nu	Nusselt number
p	Dimensional pressure, Pa
Pr	Prandtl number
q	Heat flux, W/m^2
R^2	Regression coefficient
Ra	Rayleigh number
T	Temperature, K
T_c	Temperature of cold vertical wall, K
u	x- component of velocity, m/s
v	y- component of velocity, m/s

Greek Symbols

α	Thermal diffusivity, m^2/s
β	Volume expansion coefficient, K^{-1}
θ	Dimensionless temperature
γ	Kinematic viscosity, m^2/s
ρ	Density, kg/m^3
ψ	Stream function, m^2/s

Subscripts

b	bottom wall
s	side wall

1. Introduction

Thermally induced buoyancy forces for the fluid motion and transport processes generated in an enclosure are gaining much importance because of practical significance in science and technology. The topic of natural convection in enclosures is one of the most active areas in heat transfer research today. The current study is representative of many industrial and engineering applications such as cooling of electronic equipments, meteorology, geophysics, operations and safety of nuclear reactors, energy storage, fire control, studies of air movement in attics and greenhouses, solar distillers, growth of crystals in liquids etc. Most of the early investigations of these problems are dealt by Catton [1], Jaluria [2], Ostrach [3] and Yang [4]. Sarris et al. [5] studied the effect of sinusoidal top wall temperature variations within a square cavity. It has been reported that the sinusoidal wall temperature variation produces uniform melting of metals such as glass. Buoyancy driven flows are complex because of essential coupling between the flow and thermal fields. In particular, internal flow problems are considerably more complex than external ones [6]. Electronic components are usually mounted on the vertical boards which form channels or cavities and the heat generated by the components is removed by a naturally induced flow of air [7]. Enclosures with non-uniform

temperature distributions on the walls are dealt by Erenburg et al. [8], Leong et al. [9] and Wakashima and Saitoh [10].

In the literature, investigations on natural convection heat transfer reported that the heat transfer occurs in an enclosure due to the temperature differences across the walls. Eckert and Carlson [11] have studied natural convection between two vertical plates with different temperatures in which the air is used as a working fluid. Heat transfer across the vertical layers is dealt by Emery and Chu [12]. Weinbaum [13] and Brooks and Ostrach [14] have investigated natural convection in horizontal cylinders. Shallow cavity with differentially heated end walls is dealt by Cormack [15]. The natural convection of air in enclosures or channels either uniformly heated/cooled or discretely heated have received much attention [16, 17]. Basak et al. [6] have reported the effect of temperature boundary conditions (Constant temperature and sinusoidally varying) on the bottom wall for Ra varying from 10^3 to 10^5 for both the Prandtl numbers of 0.7 and 10. The temperature of side walls as well as bottom wall affects the stratification rates and flow patterns [18].

Perusal of prior numerical investigations by Lage and Bejan [19, 20], Nicolette et al. [21], Hall et al. [22], Xia and Murthy [23] reveal that several attempts have been made to acquire a basic understanding of natural convection flows and heat transfer characteristics in enclosures. However, in most of these studies, one vertical wall of the enclosure is cooled and another one heated while the remaining top and bottom walls are insulated. Recently, Lo et al. [24] studied convection in a cavity heated from left vertical wall and cooled from opposite vertical wall with both horizontal walls insulated for temperature thermal boundary conditions using differential quadrature method. Numerical results are reported for several values of both width-to-height aspect ratio of enclosure and Raleigh number. Corcione [25] studied natural convection in a rectangular cavity heated from below and cooled from top as well as sides for variety of thermal boundary conditions. Numerical results are reported for several values of both aspect ratios of enclosure and Rayleigh numbers.

Elsherbiny et al. [26] measured natural convection heat transfer in vertical and inclined rectangular cavities where the isothermal sidewalls were at different temperatures and the end walls were perfectly conducting having a linearly varying temperature bounded by the temperature of the sidewalls. From their measurements the following correlation is presented.

$$Nu_{avg} = \max\left(\sqrt[3]{1+\left(\frac{0.193\sqrt[4]{Ra}}{1+(1800/Ra)^{1.289}}\right)^3}, 0.0605\sqrt[3]{Ra}\right) \quad (1)$$

Belkacem et al. [27] have used stream function vorticity formulation to study the natural convection of a square enclosure with sinusoidal protuberance for the Ra upto 10^6 with Pr = 0.71. Sathiyamoorthy et al. [28] have studied the effect of the temperature difference aspect ratio on natural convection in a square cavity for non-uniform thermal boundary conditions for Ra = 10^5 and for various values of Prandtl number varying from 0.01 to 10. Kandaswamy et al. [29] have studied natural convection in a square cavity in the presence of heated plate with two vertical cold walls and two horizontal adiabatic walls Grashoff number ranging from 10^3 to 10^5 for different aspect ratios and position of heated plate for Pr = 0.71.

It has been observed from the literature that most of the study on natural convection in a cavity is extended upto Ra = 10^7 and considered air as a working fluid. Basak et al. [6] have studied for Ra 10^3 to 10^5 only, for the cases of constant temperature and sinusoidally varying temperature at the bottom wall in a square cavity. However, in the present investigation, the studies are extended upto Ra = 10^7 and linearly varying temperature bottom wall is included for the range of Ra studied. Also, the present study is extended for aspect ratio 2. Recently, Basak et al. [6] have used Galerkin finite element method to study the effect of thermal boundary conditions on natural convection flows within a square cavity. In this study, the finite temperatures discontinuities are avoided at both sides by choosing non-uniform temperature distribution along the bottom wall [6].

The objective of this paper is to document the flow and heat transfer characteristics in cavities subjected to uniform, sinusoidal and linearly varying temperature at the bottom wall, symmetrically cooled side walls with uniform temperature and insulated top wall for the range of Ra from 10^3 to 10^7.

2. Mathematical Formulation

A cavity as illustrated in Fig. 1 is chosen for simulating natural convective flow and heat transfer characteristics. The cavity of length (*L)*, and height (*H)*, has a hot bottom wall with hot uniform / sinusoidal / linearly varying temperatures, two cold vertical walls are at constant temperature T_c and the top wall is adiabatic. The gravitational force is acting downwards. A buoyant flow develops because of thermally induced density gradient. Heat is transferred from the hot wall to cold wall.

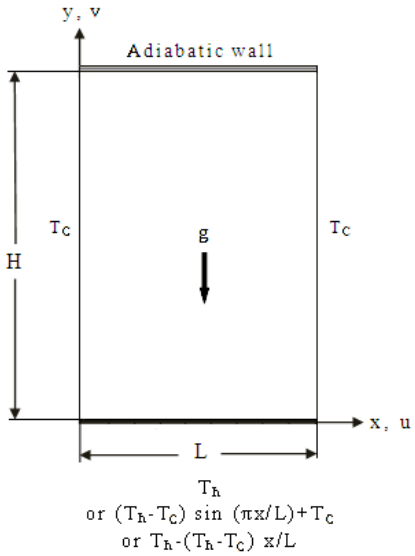

Fig. 1. Schematic Diagram of the Physical System.

The governing equations for natural convection flow are conservation of mass, momentum and energy equations [6]:

Continuity: $$\frac{\partial u}{\partial x}+\frac{\partial v}{\partial y}=0 \tag{2}$$

x-momentum: $$u\frac{\partial u}{\partial x}+v\frac{\partial u}{\partial y}=-\frac{1}{\rho}\frac{\partial p}{\partial x}+\gamma\left(\frac{\partial^2 u}{\partial x^2}+\frac{\partial^2 u}{\partial y^2}\right) \tag{3}$$

y-momentum: $$u\frac{\partial v}{\partial x}+v\frac{\partial v}{\partial y}=-\frac{1}{\rho}\frac{\partial p}{\partial y}+\gamma\left(\frac{\partial^2 v}{\partial x^2}+\frac{\partial^2 v}{\partial y^2}\right)+g\beta\left(T-T_c\right) \tag{4}$$

Energy: $$u\frac{\partial T}{\partial x}+v\frac{\partial T}{\partial y}=\alpha\left(\frac{\partial^2 T}{\partial x^2}+\frac{\partial^2 T}{\partial y^2}\right) \tag{5}$$

No-slip boundary conditions are specified at all walls.

Bottom wall: $T(x,0)=T_h$ or $T(x,0)=(T_h-T_c)\sin\left(\frac{\pi x}{L}\right)+T_c$

or $$T(x,0)=T_c+(T_h-T_c)\frac{x}{L} \tag{6}$$

Top wall: $$\frac{\partial T}{\partial y}(x,H)=0,$$

Sidewalls: $$T(0,y)=T(L,y)=T_c$$

where, *x* and *y* are the dimensional co-ordinates along horizontal and vertical directions respectively: the fluid is assumed to be Newtonian and its properties are constant. Only the Boussinesq approximation is invoked for the buoyancy term.

For the case of linear temperature variation, the boundary condition at $x = L$, is specified as the temperature value calculated by the linear temperature variation. The temperature of the cold wall at that location is ignored.

The changes of variables are as follows:

$$\theta=\frac{T-T_c}{T_h-T_c},\ \mathrm{Pr}=\frac{\nu}{\alpha},\ Ra=\frac{g\beta(T_h-T_c)L^3\,\mathrm{Pr}}{\gamma^2}\ \ldots\ldots \tag{7}$$

In the present investigation, the geometry has been created and discretized using Gambit 2.4. Fluent 6.3 CFD package is used to simulate the natural convection of air in cavities. The effect of various temperature boundary conditions at the bottom wall (like uniform / sinusoidal / linear temperature) is studied. Side cold walls are subjected to constant temperature. The top wall is adiabatic are studied for various Raleigh numbers.

3. Stream Function and Nusselt Number

3.1. Stream function

The fluid motion is displayed using the stream function Ψ obtained from velocity components u and v. The relationship between stream function, Ψ and velocity components for two dimensional flows are given by [30]:

$$u = \frac{\partial \psi}{\partial y} \text{ and } v = -\frac{\partial \psi}{\partial x} \tag{8}$$

This leads to a single equation:

$$\frac{\partial^2 \psi}{\partial x^2} + \frac{\partial^2 \psi}{\partial y^2} = \frac{\partial u}{\partial y} - \frac{\partial v}{\partial x} \tag{9}$$

Using the above definition of the stream function, the positive sign of Ψ denotes anticlockwise circulation and the clockwise circulation is represented by the negative sign of Ψ.

3.2. Nusselt number

In order to determine the local Nusselt Number, the temperature profiles are fit with quadratic, cubic and bi-quadratic polynomials and their gradients at the walls are determined. It has been observed that the temperature gradients at the surface are almost the same for all the polynomials considered. Hence only a quadratic fit is made for the temperature profiles to extract the local gradients at the walls to calculate the local heat transfer coefficients from which the local Nusselt numbers are obtained. Integrating the local Nusselt number over each side, the average Nusselt number for each side is obtained as

For bottom wall: $$Nu_{avg} = \int_0^L \mathrm{Nu_b} dx \tag{10}$$

For side wall: $$Nu_{avg} = \int_0^H \mathrm{Nu_s} dy \tag{11}$$

4. Results and Discussion

4.1. Verification of the present methodology

The grid independent study has been made with different grids and biasing of an element to yield consistent values [24]. The present methodology is compared with Lo et al. [24], in which the authors have studied for Ra = 10^3 to Ra = 10^7, for the cases of uniform temperature at vertical walls and adiabatic horizontal top and bottom walls. Different grid sizes of 31×31, 41×41, 51×51 and 61×61 uniform mesh as well as biasing have been studied. Figure 2(a) shows the convergence of the average Nusselt number at the heated surface with grid refinement for Ra = 10^5 in [24]. The grid 41×41 biasing ratio (BR) of 2 (The ratio of maximum cell to the minimum cell is 2, thus making cells finer near the wall) gave results

identical to that of 61×61 uniform mesh. In view of this, 41×41 grid with biasing ratio 2 is used in all further computations. It may be noted that Lo et al. [24] have used a uniform mesh of 31×31 for their study. However, in the present case, the study has been made for Rayleigh number ranging from 10^3 to 10^7. Sinusoidal and Linearly varying bottom wall temperature cases are also included. The average Nusselt numbers computed by the present methodology for the values of Ra ranging from 10^3 to 10^7 are compared with that in [24] in Fig. 2(b). The agreement is found to be excellent.

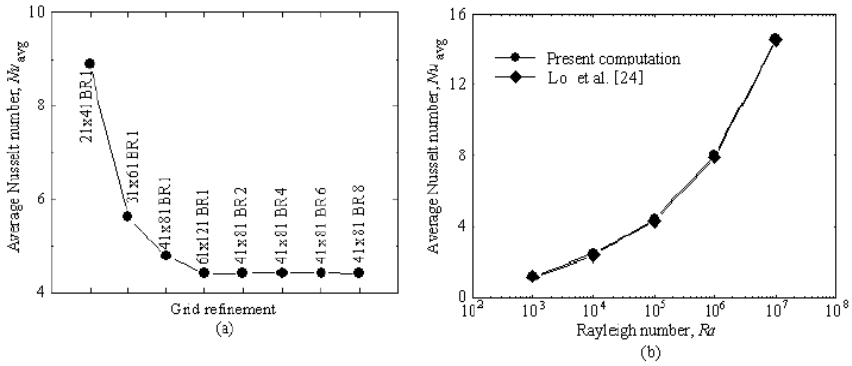

Fig. 2. Convergence of Average Nusselt Number with (a) Grid refinement and (b) Lo et al. [24].

Comparisons with local quantities of interest, such as temperature and velocities have been made with respect to the reference [6]. In addition the local Nu for both bottom and side walls for various boundary conditions have been made. A comparison of average Nu with [6] is shown in the Table 1. A comparison with available experimental results [26] is also made. The details are furnished below.

Table 1. Comparison of Average Nusselt Number with Basak et al. [6].

Ra	Bottom wall						Side wall					
	Uniform Temperature			Sinusoidal Temperature			Uniform Temperature			Sinusoidal Temperature		
	Average Nu [6]	Present study	% error	Average Nu [6]	Present study	% error	Average Nu [6]	Present study	% error	Average Nu [6]	Present study	% error
10^3	5.35	5.36	0.12	1.99	2.02	1.56	2.68	2.68	0.14	0.997	0.988	0.92
5×10^3	5.62	5.71	1.60	2.78	2.81	1.08	2.80	2.85	1.79	1.390	1.405	1.08
10^4	6.15	6.26	1.73	3.45	3.52	2.03	3.06	3.12	1.86	1.700	1.720	1.18
10^5	8.66	8.68	0.23	5.15	5.26	2.19	4.30	4.29	0.24	2.530	2.505	0.98

i) Stream functions, temperature profiles, local Nusselt number and average Nusselt number

The case of constant wall temperature at the bottom with two cold side walls, identical to the case studied in [6], has been investigated with a view to verify the present methodology. Figure 3 shows streamlines and temperature profiles of uniform temperature at bottom wall for Ra = 10^5. It is observed that there is a

good agreement between results in [6] and present one. Figure 4 shows streamlines and temperature profile for the case of bottom wall subjected to sinusoidal temperature variation for Ra = 10^5.

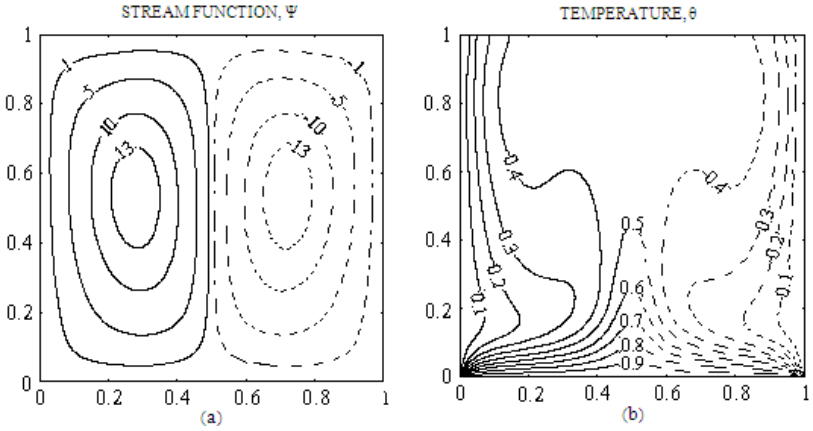

Fig. 3. Streamlines and Temperature Profiles - Uniform Temperature on Bottom Wall - Ra = 10^5.

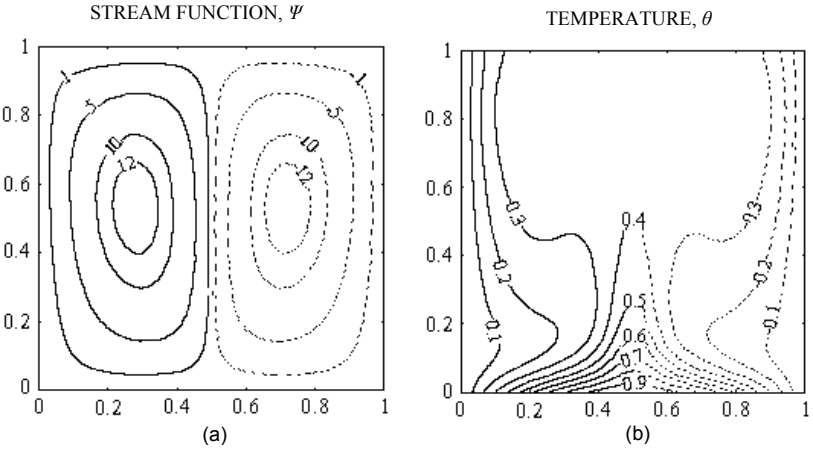

Fig. 4. Streamlines (a) and Temperature (b) Profiles - Sinusoidal Temperature on Bottom Wall - Ra = 10^5.

ii) Local Nusselt number

Next, the validation of local Nusselt number is considered. Figure 5(a) shows the comparision of local Nusselt number at the bottom wall of the present study with that in [6] for both uniform and sinusoidal temperature. It is observed from Fig. 5(a) that the local Nusselt number at the bottom wall is found to be in

excellent agrement with that in [6]. Figure 5(b) shows similar results for the side wall. Again an excellent agrement is observed between the two.

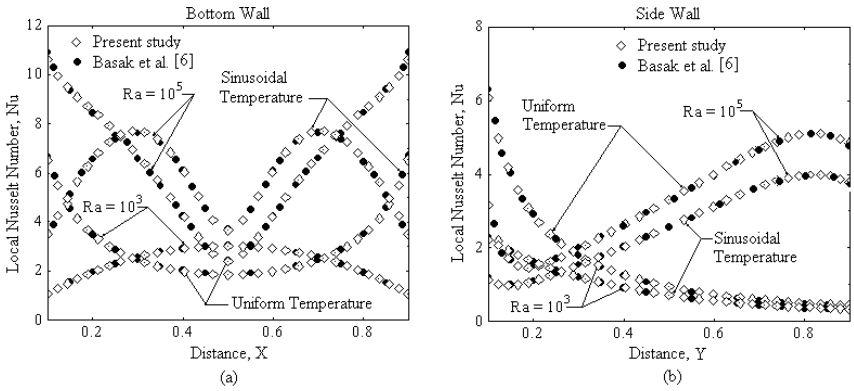

Fig. 5. Comparison of Local Nusselt number of Present Study with Basak et al. [6].

iii) Average Nusselt number

Next, a comparison of the average Nu for both bottom and side walls are made with that in [6]. Table 1 shows the comparison of variation of average Nusselt number against Rayleigh number for both bottom and side walls for constant temperature and sinusoidal variation at bottom wall. It is observed from the Table 1 that there is good agreement between the present results and that in [6] for both bottom and side walls.

iv) Verification with experimental results

Published experimental data are not available for the cavity configuration and boundary conditions similar to that undertaken in the present study. Thus, direct validation of the computations against suitable experimental data could not be performed. However, in order to validate the predictive capability and accuracy of the present code, computations are performed using the configuration and boundary conditions of the experiment conducted by [26]. They measured natural convection heat transfer in vertical and inclined rectangular cavities where the isothermal sidewalls were at different temperatures and the end walls were perfectly conducting having a linearly varying temperature bounded by the temperature of the sidewalls.

Computations are performed for one of their vertical cavity configuration with aspect ratio 5 for which they provided the experimental results in the form of a correlation for the average Nusselt number as a function of the Rayleigh number as in Eq. (1).

The average Nusselt numbers computed by the present code for values of *Ra* ranging from 10^3 to 10^7 are compared with the correlation of [26] in Fig. 6. The

agreement is found to be excellent with a maximum discrepancy of about 3.5%, which validates the present computations.

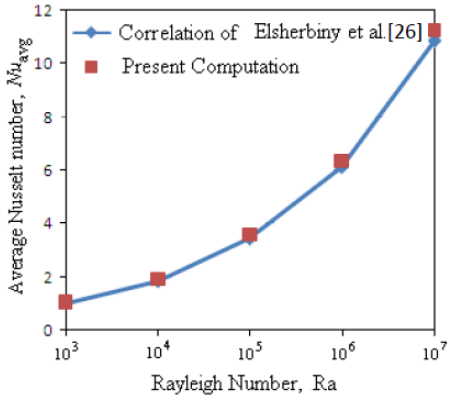

Fig. 6. Comparison of Present Average Nusselt Number with that of Elsherbiney et al. [26].

4.2. Uniform temperature at the bottom wall

The cavity used for the analysis is subjected to uniform temperature at the bottom wall. Computations are carried out for Rayleigh number ranging from 10^3 to 10^7. The aspect ratio is varied from 1 to 3. Figure 7 illustrates the stream function and isotherm contours of aspect ratio 1 and 2 for Ra = 10^3 with the bottom wall exposed to uniform temperature environment. Fluid rises up from middle portion of the bottom wall and flows down along the two vertical walls, forming two symmetric rolls with clockwise and anti-clockwise rotations inside the cavity. It has been observed that the stream functions are dragging upward in case of aspect ratio 2 as expected. For Ra = 10^3 the magnitudes of stream function are very low (ψ = 0.025 to 0.25) and the heat transfer is primarily due to conduction.

During conduction dominant heat transfer, the temperature contours are similar and occur symmetrically. In case of aspect ratio 1 (Fig. 7), the temperature contour θ = 0.1 is opened and occurs symmetrically. The temperature contours, θ = 0.2 and above are smooth curves and are generally symmetric with respect to vertical centre line. For aspect ratio 2 the temperature contours are smooth and occur symmetric about vertical centre line. Discontinuities occur at bottom corners of the cavities. The temperature contours remain invariant up to Ra < 2×10^4 (not shown).

However, the stream functions and temperature profiles for the case of 10^5 only are shown in Fig. 8. It is seen from Fig. 8(a) that, the magnitude of stream functions is double for AR = 1 compared to AR = 2. The stream functions contours are dragged vertically for AR = 2. Figure 8(b) shows the temperature profiles. The temperature profiles are spread for the entire span of the bottom wall up to θ = 0.5; symmetric about vertical line and are settling nearer to bottom wall for AR = 1. The temperature profiles θ = 0.4 and below get distorted towards side walls. For AR = 2 the temperature profiles up to θ = 0.4 are smooth curves.

However, the profiles $\theta \geq 0.6$ settle near the bottom wall. The curves $\theta = 0.3$ and lower values are concentrating nearer to the vertical cold walls.

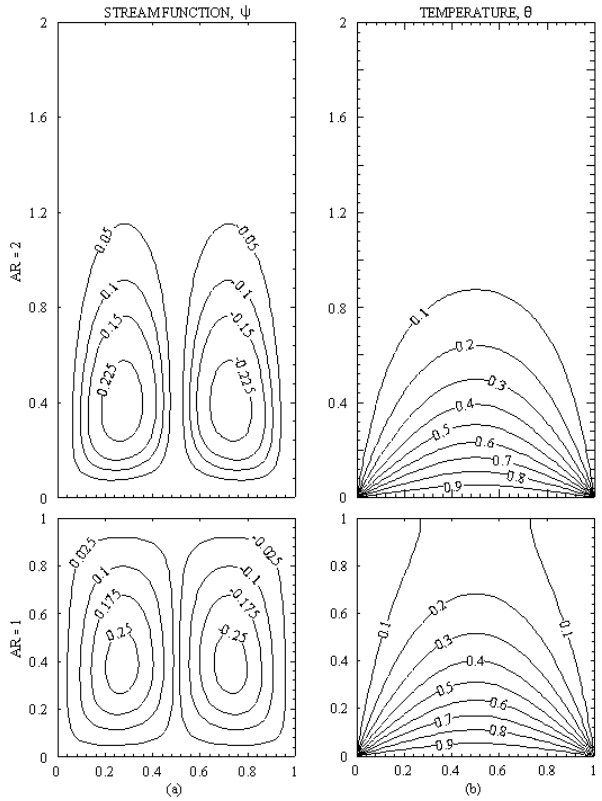

Fig. 7. Stream Lines and Temperature Profiles – Constant Temperature on Bottom Wall - Ra = 10^3.

However, the stream functions and temperature profiles for the case of 10^7 only are shown in Fig. 9. It is seen from Fig. 9(a) that, the magnitudes of stream functions are double for AR = 1 compared to aspect ratio 2. For AR = 1, the stream functions are forming circular cells at the top half of the vertical walls. Portions of the stream function contours near the cold walls are parallel. The top corners are leaning to the top corner of the cavity and bottom corners are concentrating at the middle of the bottom wall. Figure 9(b) shows the temperature profiles. For AR = 1, the temperature profiles are spread for the entire span of the bottom wall up to $\theta = 0.5$; symmetric about vertical line and are settling nearer to bottom wall. The curves $\theta = 0.4$ and lower values are concentrating nearer to the vertical cold walls. However, for AR = 2 the curves $\theta = 0.4$ and lower values raise up instead of concentrating nearer to the vertical cold walls.

Figure 10 shows the variation of local Nusselt number for both bottom wall and side walls for the Rayleigh number ranging from 10^3 to 10^7 for the uniform

temperature case. Continuous curves represent the results for AR = 2 and dashed curves are that of AR = 1. As the Rayleigh number increases the non-uniformity of the local Nusselt number at the bottom wall also increases. As expected, the local Nusselt number at any given location increases with Rayleigh number. Figure 10(a) shows the variation of local Nusselt number for bottom wall. It has been observed that the local Nusselt number increases with increase of AR. Figure 10(b) shows the variation of local Nusselt number for side wall. It can be seen from Fig. 10(b) that the local Nusselt number decreases monotonically along the side walls for Ra = 10^3 only. However, as the Ra increases to 10^5, decreasing and increasing trends are observed for local Nusselt number. Similar trends have been observed by [6] in which the analysis is made for square cavity only. But, the local Nusselt number decreases with increase of AR for a given Rayleigh number for side wall.

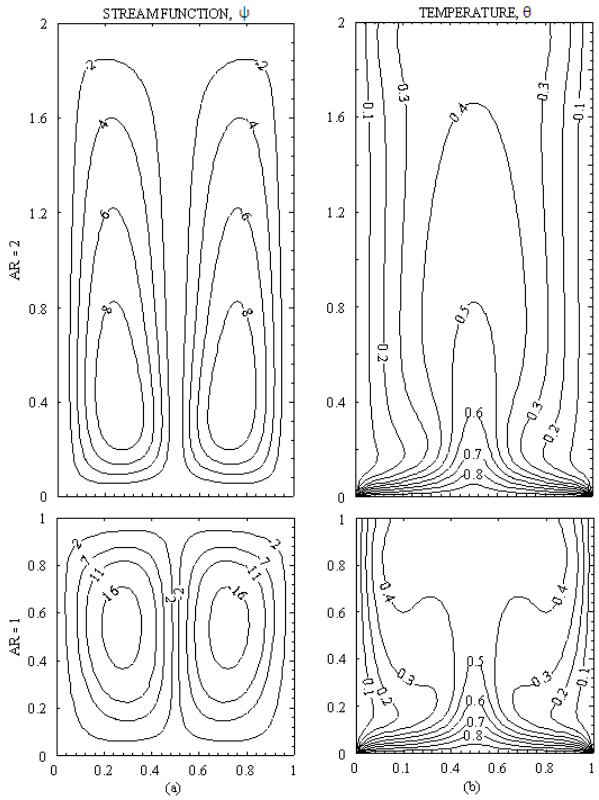

Fig. 8. Stream Lines and Temperature Profiles - Constant Temperature on Bottom Wall - Ra = 10^5.

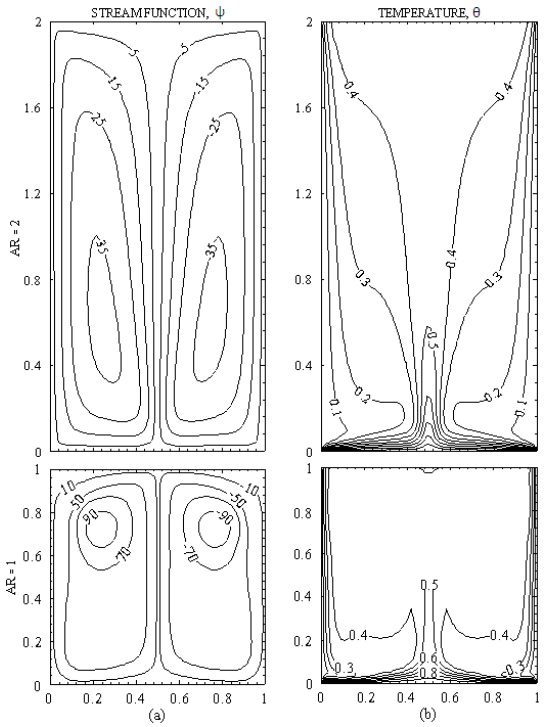

Fig. 9. Stream Lines and Temperature Profiles - Constant Temperature on Bottom Wall - Ra = 10^7.

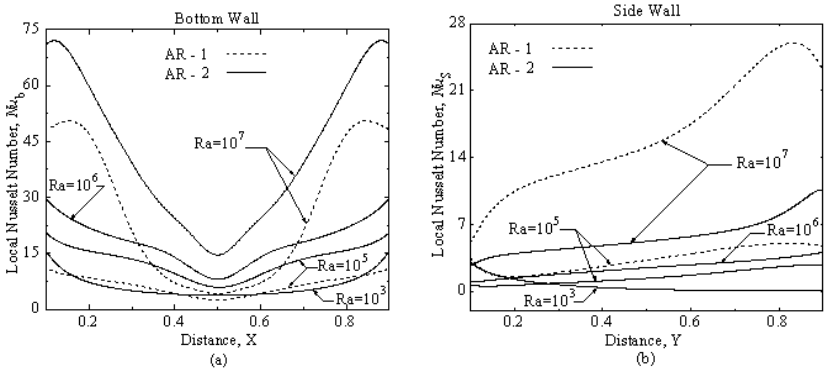

Fig. 10. Local Nusselt Numbers for Constant Temperature Case.

Figs. 11(a) and (b) show the variation of average Nusselt number for the case of uniform temperature for bottom wall and side walls respectively. It can be observed that the average Nusselt number increases with Rayleigh number as expected. It has been also observed from Figs. 11(a) and (b) that as the AR

increases, average Nusselt number for bottom wall increases but it decreases for side wall for given Rayleigh number.

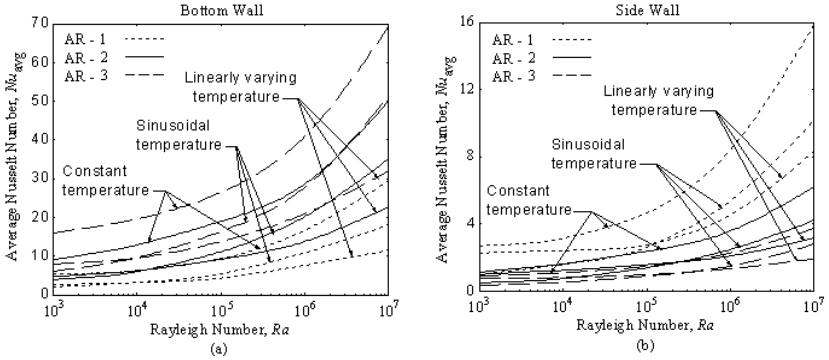

Fig. 11. Variations of Average Nusselt Number with Distance. It shows Average Nusselt Number versus Log of Rayleigh Number.

4.3. Sinusoidal temperature at the bottom wall

Next, sinusoidal temperature is used instead of uniform temperature at the bottom wall. The analysis is carried out for Rayleigh number (Ra) ranging from 10^3 to 10^7 for both AR = 1 to 3.

However, the stream functions and temperature profiles for the cases of Ra 10^5 and 10^7 are shown in Figs. 12 and 13 respectively. The magnitudes of the stream functions for Ra = 10^7 shown in Fig. 13(a) are high compared to those for Ra = 10^5 (Fig. 12) and the stream lines are dragging vertically for AR = 2 as expected. Figures 12(b) and 13(b) show the temperature contours for Ra = 10^5 and 10^7 respectively. 70% of the temperature contours are crowded near the bottom wall and spread along the length of the bottom wall for both AR = 1 and 2.

Figure 14(a) shows the variation of local Nusselt number on bottom wall. The local Nusselt number is symmetrical about the centre of the bottom vertical line. As expected, the variation is less up to Ra = 4×10^4 due to conduction dominance for AR = 1 and Ra = 5×10^4 for AR = 2. The local Nusselt number increases with increase of Ra at the centre of the bottom wall and reduces towards the cold walls as expected. However, the local Nusselt number decreases with increases of AR. Figure 14(b) shows the variation of local Nusselt number for the side wall. For Ra = 10^3 and 10^4, local Nusselt number decreases monotonically along the length. For Ra = 10^5 and Ra = 10^6, slightly decreasing and increasing trend is observed. For other values of Ra, local Nusselt number increases first and then decreases near the right side wall. For side wall, the Local Nusselt number decreases with increase of AR. In case of heating of an isolated vertical plate with constant temperature, the Nusselt number is maximum at the bottom and monotonically decreases as the height increases. From Fig. 14(b) same trend is observed for Ra = 10^3 for the side wall. However, for Ra = 10^5 and 10^6 it is increasing almost linearly and flat at the end as the top wall is adiabatic. This may be due to the increased convection currents at the centre due to increase in Rayleigh number and these convection currents push the heated fluid towards the side walls (as

seen in Fig. 12(b) with AR = 1), increasing the transfer of heat which leads to increase in Nu along the height. For Ra = 10^7, with aspect ratio 1, Nusselt number increases, reaches to a peak and again it reduces for the side wall.

Figure 11 also shows the variation of average Nusselt number against Rayleigh number. It can be seen that the values are lower than those of uniform wall temperature at bottom wall for AR = 1 to 3. Figure 11 also shows that average Nusselt number increases with increase of AR for bottom wall and decreases for side wall for a given Rayleigh number. It is well known that when the gap between top and bottom wall is very small in a cavity, only conduction mode heat transfer will take place. As the height of the top wall increases, convection current sets in and thus heat transfer increases. In the present case when the AR increases, the resistance for convection current will decrease and thus the heat transfer increases at the bottom wall. The significance of this is that, increase in Nu, for a given Ra at the bottom wall is obtained by increasing the AR.

In the case of side wall, for a given Ra, as the AR increases the fluid will get more cooled at the top as observed in Fig. 12(b) for AR = 2. This cooled fluid will start flowing along the side walls in a downward direction as seen in Fig. 12(a) for AR = 2. This reduces the heat transfer from top to bottom as indicated in Fig. 14(b) for Ra other than 10^3 (conduction dominated). This leads to reduction in Nu for the side wall as AR increases for convection dominated flows. For the side wall, in order to maintain the same Nu as that of AR = 1, it is necessary to increase Ra when AR increases to 2.

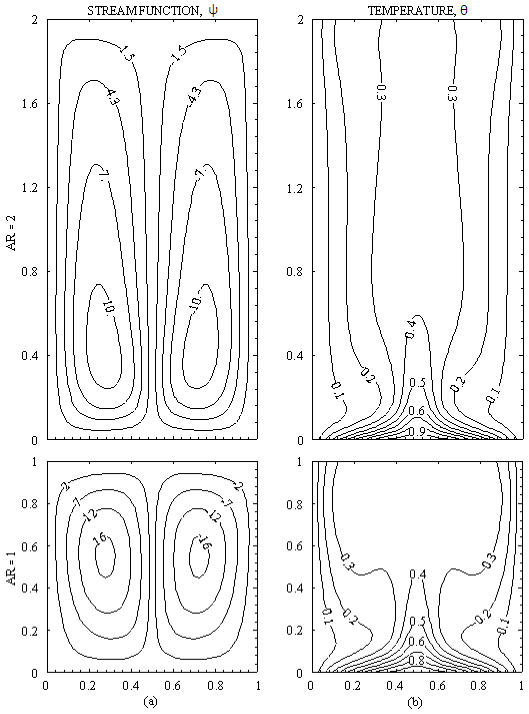

Fig. 12. Stream Lines and Temperature Profiles - Sinusoidal Temperature on Bottom Wall - Ra = 10^5.

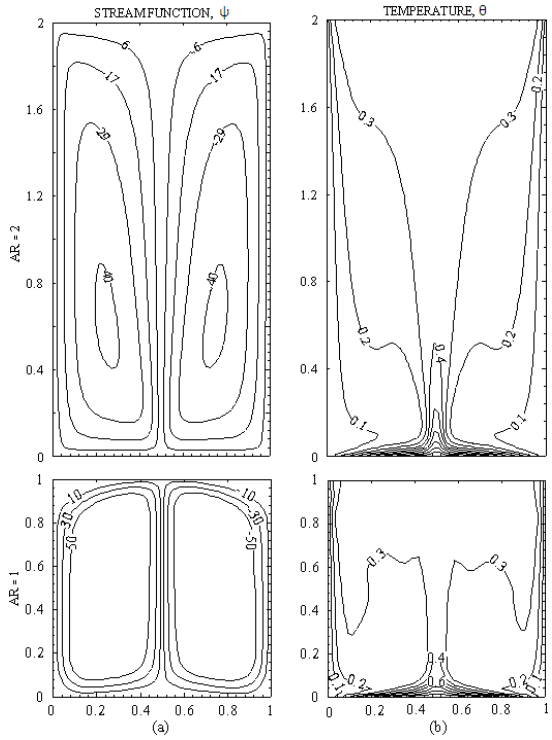

Fig. 13. Stream Lines and Temperature Profiles - Sinusoidal Temperature on Bottom Wall - Ra = 10^7.

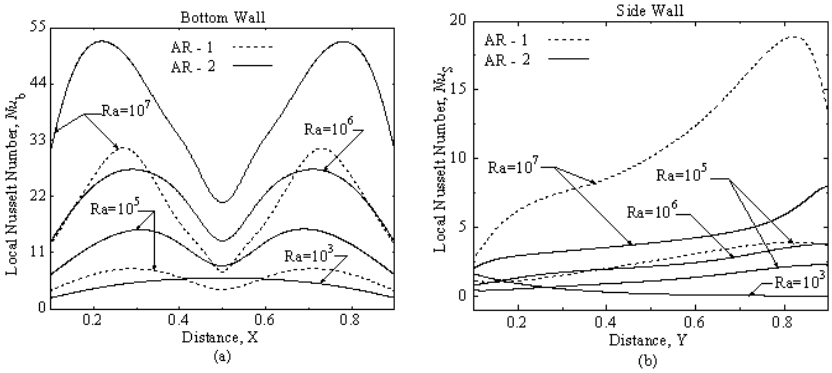

Fig. 14. Local Nusselt Numbers for Sinusoidal Temperature Case.

4.4. Linearly varying temperature at the bottom wall

Stream function contours and isotherms are shown in Figs. 15 and 16 for Ra = 10^5 and 10^7 when the bottom wall is subjected to linearly varying temperature. A

finite discontinuity in Dirichlet type boundary conditions exists for constant temperature at both side walls and bottom wall. In contrast, the linearly varying temperature removes the singularities at one edge of the bottom wall and profiles are not symmetric about central vertical line. The temperature at bottom wall is varying linearly and a maximum temperature occurs at the right wall. Figure 15 shows the streamlines and temperature profiles for Ra = 10^5. For AR = 1, the left side cells are extended towards right side, resulting in smaller cells on the right. However, in case of AR = 2 the right side cells are extended at the middle of the side wall. The Left cells are dragging to right at top and bottom of the cavity. The left inner cells tend to split the cells at top and bottom. It can be observed that the temperature contours are not similar with $\theta = 0.1$ and 0.2 and are not symmetrical near side walls of the enclosure as that of the uniform temperature case for AR = 1. The other temperature contours, for $\theta = 0.3$ and above are smooth curves. For AR = 2 temperature contour of $\theta = 0.1$ is not a smooth curve.

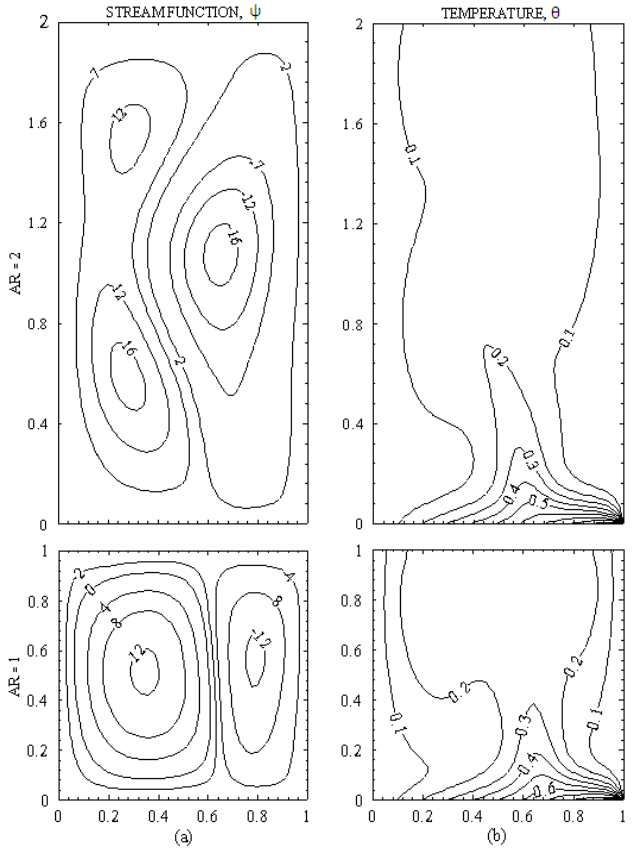

Fig. 15. Stream Lines and Temperature Profiles - Linearly Varying Temperature on Bottom Wall - Ra = 10^5.

Figure 16 shows the streamlines and temperature profiles for Ra = 10^7. It can be observed that the right cell moves to left in the top whereas left cell extends to right in the bottom for AR = 1 and are extended vertically for AR = 2. Stream function values have increased substantially showing strong circulations. However, the magnitudes of stream functions are very small for AR = 2 compared to those of AR = 1. Figure 16(b) shows a distorted temperature profiles due to convection. It can be seen that the temperature profiles concentrate towards right bottom corner.

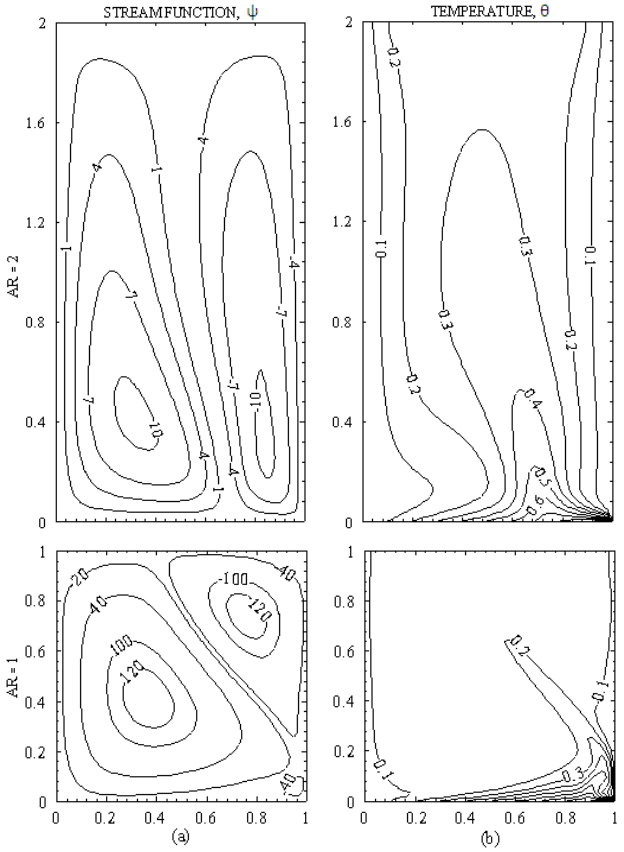

Fig. 16. Stream Lines and Temperature Profiles - Linearly Varying Temperature on Bottom Wall - Ra = 10^7.

Figure 17 shows the variation of local Nusselt number along the bottom and side walls. For Ra = 10^3, the local Nusselt number increases monotonically for bottom wall. For Ra = 10^5 and 10^7 they show increasing, decreasing and again increasing trend for AR = 1. However, for AR = 2 shows decreasing, increasing and decreasing trends. For side walls with Ra = 10^3, the local Nusselt number decreases monotonically for both AR = 1 and 2. For AR = 1 and Ra = 10^5, the local Nusselt number decreases and then increases. But, for Ra = 10^7, local Nusselt number increases and then decreases. For AR = 2, the local Nusselt

numbers behave in zigzag manner. Figure 11 also shows the variation of average Nusselt number with Rayleigh number. For linear varying temperature on the bottom wall, the variation of average Nusselt number increases with increase of Rayleigh number as expected.

The overall effect on the heat transfer rate is shown in Figs. 11(a) and 11(b) in which the distributions of the average Nusselt number for both bottom and side walls are shown respectively. They are plotted against the logarithmic Rayleigh number. A least square curve is fitted and the overall error is within 3%. The error involved is tabulated in the Table 2. It has been observed from the table that, the error involved increased with increase of Rayleigh number. The correlations derived in the present study are given in Table 2.

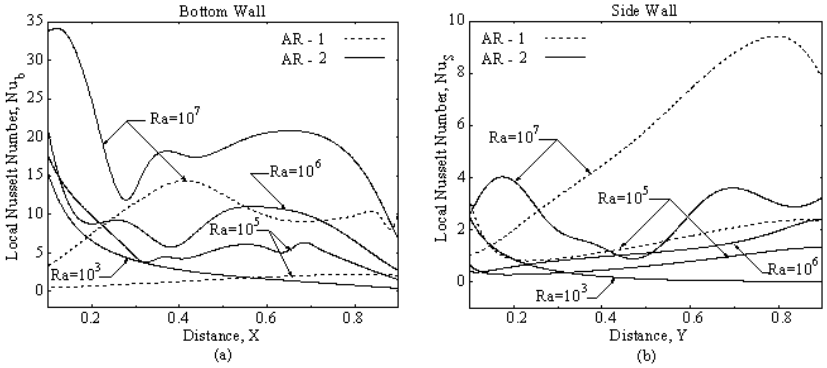

Fig. 17. Local Nusselt Numbers for Linearly Varying Temperature Case.

Table 2. Correlation of Nusselt Number with Rayleigh Number for Various Aspect Ratios.

Heating type	Rayleigh number range	Aspect ratio (AR)	Bottom Wall			Side Wall		
			Correlation	R^2	% error	Correlation	R^2	% error
Uniform temperature	5×10^3 to 10^5	1	$Nu_{avg} = 1.611Ra^{0.145}$	1.000	< 1.0	$Nu_{avg} = 0.885Ra^{0.136}$	0.999	< 1.0
		2	$Nu_{avg} = 2.653Ra^{0.17}$	0.999	< 0.5	$Nu_{avg} = 0.337Ra^{0.168}$	0.999	< 1.0
	10^5 to 10^7	1	$Nu_{avg} = 0.397Ra^{0.267}$	1.000	< 2.0	$Nu_{avg} = 0.145Ra^{0.289}$	0.999	< 2.0
		2	$Nu_{avg} = 1.574Ra^{0.213}$	0.999	< 1.5	$Nu_{avg} = 0.206Ra^{0.210}$	0.999	< 1.5
	5×10^3 to 10^7	1	$Nu_{avg} = 0.799Ra^{0.219}$	0.996	< 3.0	$Nu_{avg} = 0.347Ra^{0.229}$	0.997	< 3.0
		2	$Nu_{avg} = 2.058Ra^{0.195}$	0.997	< 3.0	$Nu_{avg} = 0.257Ra^{0.195}$	0.997	< 3.0
	8×10^4 to 10^7	3	$Nu_{avg} = 2.085Ra^{0.214}$	0.993	< 3.0	$Nu_{avg} = 0.125Ra^{0.208}$	0.994	< 2.5
Sinusoidal temperature	2×10^4 to 10^5	1	$Nu_{avg} = 0.298Ra^{0.249}$	0.999	< 1.0	$Nu_{avg} = 0.154Ra^{0.242}$	0.999	< 1.0
		2	$Nu_{avg} = 0.581Ra^{0.251}$	0.999	< 0.5	$Nu_{avg} = 0.032Ra^{0.298}$	0.999	< 0.5
	10^5 to 10^7	1	$Nu_{avg} = 0.272Ra^{0.261}$	0.998	< 2.0	$Nu_{avg} = 0.072Ra^{0.305}$	0.999	< 2.0
		2	$Nu_{avg} = 0.508Ra^{0.261}$	0.999	< 1.5	$Nu_{avg} = 0.031Ra^{0.302}$	1.000	< 1.5
	2×10^4 to 10^7	1	$Nu_{avg} = 0.248Ra^{0.267}$	0.999	< 2.9	$Nu_{avg} = 0.088Ra^{0.292}$	0.998	< 3.0
		2	$Nu_{avg} = 0.550Ra^{0.256}$	0.999	< 1.5	$Nu_{avg} = 0.031Ra^{0.301}$	1.000	< 1.5
	10^4 to 10^7	3	$Nu_{avg} = 0.913Ra^{0.246}$	0.995	< 3.0	$Nu_{avg} = 0.048Ra^{0.247}$	0.994	< 3.0
Linearly varying temperature	10^5 to 10^7	1	$Nu_{avg} = 0.374Ra^{0.215}$	0.998	< 3.0	$Nu_{avg} = 0.050Ra^{0.287}$	0.998	< 3.0
	2×10^4 to 10^7		$Nu_{avg} = 0.378Ra^{0.212}$	0.997	< 3.0	$Nu_{avg} = 0.053Ra^{0.284}$	0.998	< 3.0
	10^5 to 10^7	2	$Nu_{avg} = 1.201Ra^{0.172}$	0.998	< 1.0	$Nu_{avg} = 0.326Ra^{0.135}$	0.999	< 0.5
	10^4 to 10^7	3	$Nu_{avg} = 1.642Ra^{0.183}$	0.998	< 1.0	$Nu_{avg} = 0.194Ra^{0.140}$	0.994	< 2.5

4.5. Correlations of average Nusselt number with Rayleigh number

i) Uniform temperature:

In the present study, for AR = 1, the correlation obtained for Ra = 5×10^3 to 10^5 is different from that in [6] utmost by 0.675%. The maximum error involved in correlating average Nusselt number with Rayleigh number is less than 2% in the range of Ra = 10^5 to 10^7. For the combined case i.e. for Rayleigh number ranging from 5×10^3 to 10^7, the utmost error is 3%.

ii) Sinusoidal temperature:

The correlation presented in Table 2 is for sinusoidal temperature variation at bottom wall and is very close to that of [6] with a maximum error of 1% in which studies are limited to AR = 1. However, the error increases to a maximum of 3% when Ra ranges from 2×10^4 to 10^7. It is seen from Table 1 that for AR = 2, the error involved does not exceed 1.5%.

iii) Linearly varying temperature:

The correlation presented in Table 2 is for aspect ratios 1 to 3. For Aspect ratio 1 and linearly varying temperature at bottom wall in the range of Ra = 10^5 to 10^7, a maximum error of 3% is obtained. It is also observed that when the range of Ra is from 2×10^4 to 10^7 the maximum error is 3% for the bottom wall. However, for the side wall the maximum error is seen to be 3%. For the case of AR = 3 the maximum error in using the correlation for the range of Ra varying from 10^4 to 10^7 is utmost 1% for the bottom wall whereas it is 2.5% for the side wall.

5. Conclusions

The effect of different temperature boundary conditions like uniform, sinusoidal and linearly varying temperature at the bottom wall for AR = 1 to 3 have been investigated. The top wall is adiabatic and side walls are maintained at constant temperature. The following conclusions have been observed during the present study.

- For uniform temperature case the conduction dominant heat transfer mode occurs up to Ra $\leq 5\times10^3$, whereas it occurs at Ra $\leq 2\times10^4$ for sinusoidal cases, same as observed in the literature.
- The contours of stream functions and isotherms are symmetric about centre of vertical line for uniform and sinusoidal temperature cases, but they are not symmetric for linearly varying temperature case.
- The magnitude of stream functions is more for uniform temperature case compared to other two cases for AR = 1.
- The average Nusselt number increases monotonically with increase of both Ra and AR at bottom wall whereas it is decreasing for side wall with increase of AR.
- It has been observed that the average Nusselt number for the case of uniform bottom wall is more than that of sinusoidally and linearly varying temperature profile at the hot and cold walls.
- For a given Ra, the increase in Nu can be obtained by increasing the AR for bottom wall.

Acknowledgements

The authors thank the reviewers for their critical comments which improved the paper.

References

1. Catton, I. (1978). Natural convection in enclosures. *Proceedings of 6th Int. Heat Transfer Conference, Toronto,* 6, 13-43.
2. Jaluria, Y. (1980). *Natural convection heat and mass transfer*. Pergamon, Oxford, 209-235.
3. Ostrach, S. (1988). Natural convection in enclosures. *Journal of Heat Transfer,* 110(4b), 1175-1190.
4. Yang, K.T. (1988). Transitions and bifurcations in laminar buoyant flows in confined enclosures. *Journal of Heat Transfer,* 110(4b), 1191-1204.
5. Sarris, I.E.; Lekakis, I.; and Vlachos, N.S. (2002). Natural convection in a 2D enclosure with sinusoidal upper wall temperature. *Numerical Heat Transfer A*, 42(5), 513-530.
6. Basak, T.; Roy, S.; and Balakrishnan, A.R. (2006). Effects of thermal boundary conditions on natural convection flows with in a square cavity. *International Journal of Heat and Mass Transfer*, 49(23-24), 4525-4535.
7. Dehghan, A.A.; and Behnia, M. (1996). Combined natural convection-conduction and radiation heat transfer in a discretely heated open cavity. *Transactions of ASME*, *Journal of Heat Transfer*, 118(1), 56-64.
8. Erenburg, V.; Gelfgat, A.Y.; Kit, E.; Bar-Yoseph, P.Z.; and Solan, A. (2003). Multiple states, stability and bifurcations of natural convection in a rectangular cavity with partially heated vertical walls. *Journal of Fluid Mechanics,* 492, 63-89.
9. Leong, W.H.; Hollands, K.G.T.; and Brunger, A.P. (1998). Experimental Nusselt numbers for a cubical-cavity benchmark problem in natural convection. *International Journal of Heat and Mass Transfer,* 42(11), 1979-1989.
10. Wakashima, S.; and Saitoh, T.S. (2004). Benchmark solutions for natural convection in a cubic cavity using the high-order time-space methods. *International Journal of Heat and Mass Transfer,* 47(4), 853-864.
11. Eckert, E.R.G.; and Carlson, W.O. (1961). Natural convection in an air layer enclosed between two vertical plates with different temperatures. *International Journal of Heat and Mass Transfer*, 2(1-2), 106-120.
12. Emery, A.; and Chu, N.C. (1965). Heat transfer across vertical layers. *Transactions of ASME*, *Journal of Heat Transfer,* 87(1), 110-116.
13. Weinbaum, S. (1964). Natural convection in horizontal cylinders. *Journal of Fluid Mechanics,* 18(3), 409-448.
14. Brooks, I.H.; and Ostrach, S. (1970). An experimental investigation of natural convection in a horizontal cylinder. *Journal of Fluid Mechanics*, 44(3), 545-561.
15. Cormack, D. E.; Leal, L. G.; and Seinfeld, J. H. (1974). Natural convection in shallow cavity with differentially heated end walls. Part 2, Numerical solutions. *Journal of Fluid Mechanics,* 65(2), 231-246.

16. Chadwick, L.; Webb, B.M.; and Ricci, R. (1991). Natural convection from two dimensional discrete heat sources in a rectangular enclosure. *International Journal of Heat and Mass Transfer,* 34(7), 1679-1693.
17. Ahmed, G.R.; and Yovanovich, M.M. (1991). Influence of discrete heat source location on convection heat transfer in a vertical square enclosure. *ASME Journal of Electronic Packaging*, 113(3), 268-274.
18. Dixit, H. N.; and Babu, V. (2006). Simulation of high Rayleigh number natural convection in a square cavity using the lattice Boltzmann method. *International Journal of Heat and Mass Transfer*, 49(3-4), 727-739.
19. Lage, J.L.; and Bejan, A. (1991). The Ra-Pr domain of laminar natural convection in an enclosure heated from the sides. *Numerical Heat Transfer Part A,* 19(1), 21-41.
20. Lage, J.L.; and Bejan, A. (1993). The resonance of natural convection in an enclosure heated periodically from the side. *International Journal of Heat and Mass Transfer*, 36(8), 2027-2038.
21. Nicolette, V. F.; Yang, K.T.; and Lloyd, J.R. (1985). Transient cooling by natural convection in a two-dimensional square enclosure. *International Journal of Heat and Mass Transfer*, 28(9), 1721-1732.
22. Hall, J.D.; Bejan, A.; and Chaddock, J.B. (1988). Transient natural convection in a rectangular enclosure with one heated side wall. *International Journal of Heat and Fluid Flow*, 9(4), 396-404.
23. Xia, C.; and Murthy, J.Y. (2002). Buoyancy-driven flow transitions in deep cavities heated from below. *Transactions of ASME*, *Journal of Heat Transfer*, 124(4), 650-659.
24. Lo, D.C.; Young, D.L.; and Tsai, C.C. (2007). High resolution of 2D natural convection in a cavity by the DQ method. *Journal of Computational and Applied Mathematics,* 203(1), 219-236.
25. Corcione, M. (2003). Effects of the thermal boundary conditions at the sidewalls upon natural convection in rectangular enclosures heated from below and cooled from above. *International Journal of Thermal Sciences*, 42(2), 199-208.
26. Elsherbiny, S.M.; Raithby, G.D.; and Hollands, K.G.T. (1982). Heat transfer by natural convection across vertical and inclined air layers. *Transactions of ASME*, *Journal of Heat Transfer*, 104(1), 96-102.
27. Belkacem, A.; Omar, H.; and Mebrouk, R. (2006). Stream function/vorticity formulation to study the cavity flows by unstructured grid method. *International Journal of Applied Engineering Research*, 1(3), 315-329.
28. Sathiyamoorthy, M.; Basak, T.; Roy, S.; and Mahanti, N.C. (2007). Effect of the temperature difference aspect ratio on natural convection in a square cavity for non-uniform thermal boundary conditions. *Transactions of ASME*, *Journal of Heat Transfer*, 129(12), 1723-1728.
29. Kandaswamy, P.; Lee, J.; and Abdul Hakeem, A.K. (2007). Natural convection in a square cavity in the presence of heated plate. *Nonlinear Analysis: Modelling and Control*, 12(2), 203–212.
30. Batchelor, G.K. (1993). *An introduction to fluid dynamics*. Cambridge University Press, Cambridge, UK.